A new algorithm for 2D Region of Interest Tomography

G. Van Gompel, G. Tisson, D. Van Dyck, J. Sijbers

Vision Lab, University of Antwerp, Groenenborgerlaan 171, B-2020 Antwerp, Belgium.

ABSTRACT

In this paper, we develop a new algorithm that enables the reconstruction of a region of interest (ROI) in X-ray Computed Tomography (CT), in case only a local region of the object is to be imaged. The method uses a Gaussian window function in order to reduce the X-ray attenuation from the region outside the ROI. The method uses almost completely local data and reduces the amount of exposure significantly. Many algorithms can be easily combined with our algorithm in order to improve the reconstruction quality. The main goal of this work is to reduce the bias in order to allow quantitative analysis of the CT-images.

1. INTRODUCTION

ROI-tomography deals with the problem of reconstructing a specific part of an object from truncated projections (consider the ROI always fully detected).
The problem of reconstructing an image from a complete set of projections is to compute the image from its Radon Transform, i.e. a complete set of line integrals $p_\theta(r)$, defined as:

$$p_\theta(r) = \int_{-\infty}^{\infty}\int_{-\infty}^{\infty} f(x,y)\delta(r - x\cos\theta - y\sin\theta)dxdy \tag{1}$$

The inverse Radon transform is usually performed with the Filtered Backprojection algorithm (FBP), which is based on the Fourier slice theorem* [2]. The FBP algorithm contains two steps: a filtering part, in which the projections are convolved with a rampfilter, and a reconstruction part in which the filtered projections are backprojected along the projection directions. The quality of a reconstruction from complete projections with FBP is generally satisfactory, depending on the number of angles and sampling points [2].
The main problem of reconstructing a 2D ROI from truncated projections is the non-locality of the Radon Transform. Indeed, the inverse Radon Transform in even dimensions globally depends upon line integrals of the object function. The effect of this non-local operation on truncated projections is an asymptotic bias, which is large at the edges of the ROI, and becomes smaller towards its center [3, 11]. Due to the non-locality, which is reflected in the filter in the FBP algorithm, one is forced to use full exposures.

If the ROI problem can be adequately solved, it has a lot of applications. One important application in cone-beam tomography is the possibility of enlarging a part of an object by moving the object towards the source so that the ROI covers the field of view of the detector. In this case one has an optimal resolution of the ROI. ROI tomography also permits a significant reduction of the exposure time, dose, and computation time.

Several researchers have proposed algorithms that improve the quality of the reconstruction of a ROI. Most of these algorithms are based on data completion [4–10]. Completion of truncated projections with a smooth function (elimination of the edge artifacts) already improves the reconstruction significantly. Further improvement can be obtained by acquiring extra information of the region outside the ROI, e.g. the truncated projections of the high resolution scan can be combined with a second, low resolution scan of the whole object. The question is then how much information is needed for a satisfactory result.

Send correspondence to:
gert.vangompel@ua.ac.be
greg.tisson@ua.ac.be

*The Fourier slice theorem states that the 1D Fourier transform of a parallel projection is equal to a slice of the 2D Fourier transform of the original object. It follows that, given the Fourier transform of the projection data, it is possible to estimate the object by means of a 2D inverse Fourier transform.

Medical Imaging 2004: Image Processing, edited by
J. Michael Fitzpatrick, Milan Sonka, Proceedings of SPIE Vol. 5370
(SPIE, Bellingham, WA, 2004) · 1605-7422/04/$15 · doi: 10.1117/12.536685

Intuitively, the 2D ROI problem can be approached in two different ways. From the perspective of reconstructing the entire object, some of the data from the region outside the ROI are missing. However, from the perspective of reconstructing only the ROI, the x-rays penetrate other portions of the object as well, thus the collected data are corrupted by the unknown structures outside the ROI. The corruption increases for a decreasing size of the ROI, and when the structures surrounding the ROI are denser. This result forms the foundation of our algorithm.
As mentioned above, most ROI reconstruction techniques pursue data completion [4–10]. Our technique aims elimination of the extra information outside the ROI. We will present a method that manipulates the truncated projections so that these can be interpreted as originating from the product of the object function with a 2D Gaussian window function. The main effect of this window is a reduction of the influence of the data outside the ROI. In this paper, we investigate the algorithm numerically, and derive an error estimate. The algorithm is described in 2D in which we modify the use of the standard FBP for a parallel geometry. However, the algorithm can be easily extended to realistic 3D cone-beam scanning configurations, which use FBP-based reconstruction algorithms, and can be applied to visualize objects bigger than the field of view.

2. METHOD

2.1. Idea

There are two situations that permit a perfect reconstruction of the ROI: all information of the entire object is available, or only the information originating from the ROI. Truncated projections don't correspond to one of these two situations, because they do not contain the full information of the object, and they contain more information than just that of the ROI. Our technique pursues elimination of the extra information outside the ROI. This can be done by multiplying the object with a window function. However, in a real experiment, the object function is unknown and we only have the indirect truncated projections. But according to the Fourier Slice Theorem, the dual operation in Fourier space can be approximately calculated from the truncated projections. This means that the 2D Fourier transform of the truncated projections (under equally spaced angles in the plane), is convolved with the Fourier transform of the window function. The trick is now to

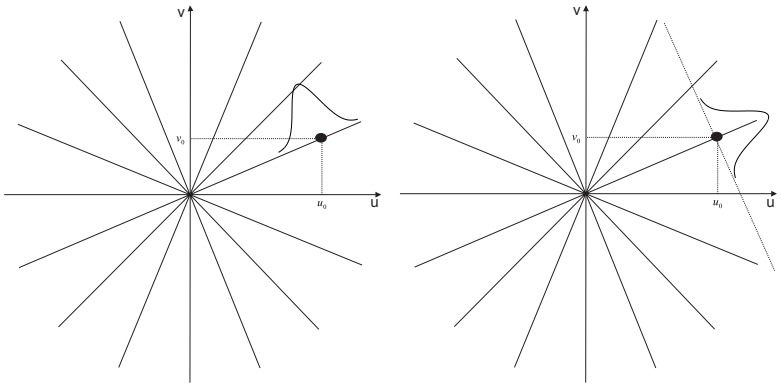

(a) radial convolution (b) angular convolution

Figure 1. split of the 2D convolution in a radial (a)and an angular (b) convolution

use a 2D spherical Gaussian window, since this can be factorised in two 1D Gaussian functions at any two orthogonal axes, which is consistent with the backprojection method. The first step is the radial convolution in Fourier space of the projections and a 1D Gaussian window, since the Fourier transform of a Gaussian function remains a Gaussian function. The analogon in real space is multiplication with a 1D Gaussian function. Next,

we need to perform the angular convolution in Fourier space†. However, it is more convenient to perform this operation in real space, since interpolation in Fourier space easily leads to erroneous results. So the object is first reconstructed with the filtered backprojection. Then, this reconstructed ROI is reprojected with a 1D Gaussian weight factor which corresponds with the position of the ROI, since this operation corresponds with the angular convolution in frequency space. Again, the FBP algorithm is applied and afterwards normalized by dividing the ROI by the 2D Gaussian.

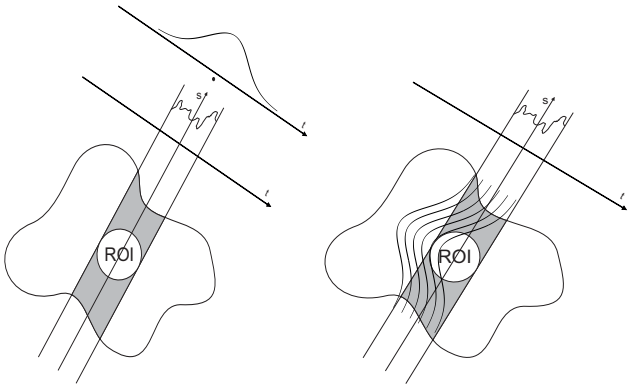

(a) radial (b) angular

Figure 2. meaning of the two 1D multiplications in real space

Summary

1. Multiply every projection with a 1D Gaussian function (see figure 2.1 a).
2. Reconstruct the object with FBP.
3. Perform a weighted Radon transform with a 1D Gaussian function as a weighting function (see figure 2.1 b).
4. Again, reconstruct with FBP.
5. Divide the reconstructed object by the 2D Gaussian function.

2.2. Discussion

Because a Gaussian function can be factorised in two 1D Gaussian functions at any pair of orthogonal axes, we can split the 2D convolution in two 1D convolutions. This split is only correct when the pair of orthogonal axes is the same for every point in which the convolution is calculated. This is not the case in our algorithm. The question is now what the consequences are for the reconstruction.

We describe the problem in the frequency space. The first step is a convolution in the radial direction of a Fourier transformed projection $P_{\theta'}(k')$ with a 1D Fourier transformed Gaussian function $G(k')$

$$P^R_{\theta'}(k') = \int_{-\infty}^{\infty} G(\epsilon') P_{\theta'}(k' - \epsilon') d\epsilon', \tag{2}$$

with $P^R_{\theta'}(k')$ the result of this convolution. According to the Fourier slice theorem, this equals

$$F^R(k' \cos\theta', k' \sin\theta') = \int_{-\infty}^{\infty} G(\epsilon') F\left((k' - \epsilon') \cos\theta', (k' - \epsilon') \sin\theta'\right) d\epsilon', \tag{3}$$

†The use of 'angular' is not completely correct. With 'angular convolution' we mean a convolution perpendicular to the radial direction along a straight line, not along a concentric line according to the strict meaning of the word

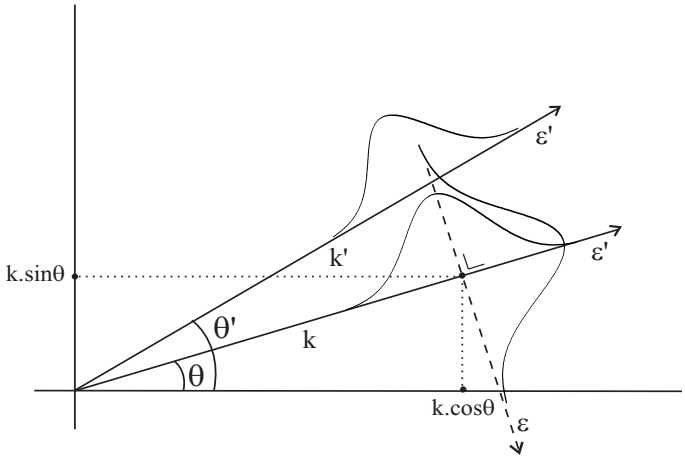

Figure 3. visualisation of the symbols

with $F^R(k'\cos\theta', k'\sin\theta')$ and $F(k'\cos\theta', k'\sin\theta')$ the Fourier transformed and the radially convolved Fourier transformed object function, respectively. The second convolution, perpendicular to the radial direction, can then be written as

$$F^{RA}(k\cos\theta, k\sin\theta) = \int G(\epsilon) F^R(k\cos\theta - \epsilon\sin\theta, k\sin\theta + \epsilon\cos\theta) d\epsilon, \tag{4}$$

with $F^{RA}(k\cos\theta, k\sin\theta)$ the result of this angular convolution. Moreover, $F^R(k\cos\theta - \epsilon\sin\theta, k\sin\theta + \epsilon\cos\theta)$ can be written as $F^R(k'\cos\theta', k'\sin\theta')$ with

$$\begin{aligned} k' &= \sqrt{k^2 + \epsilon^2} \\ \cos\theta' &= \frac{k\cos\theta - \epsilon\sin\theta}{\sqrt{k^2+\epsilon^2}} \\ \sin\theta' &= \frac{k\sin\theta + \epsilon\cos\theta}{\sqrt{k^2+\epsilon^2}}. \end{aligned} \tag{5}$$

Substitution of (3) and (5) in (4) yields

$$\begin{aligned} F^{RA}(k\cos\theta, k\sin\theta) = \iint G(\epsilon)G(\epsilon') F\left[k\cos\theta - \epsilon\sin\theta - \epsilon' \frac{k\cos\theta - \epsilon\sin\theta}{\sqrt{k^2+\epsilon^2}}, \right. \\ \left. k\sin\theta + \epsilon\cos\theta - \epsilon' \frac{k\sin\theta + \epsilon\cos\theta}{\sqrt{k^2+\epsilon^2}} \right] d\epsilon\, d\epsilon'. \end{aligned} \tag{6}$$

k small (near the origin)

When k is small compared to the width of the Gaussian function, then the angular convolution is performed over an interval which contains many points whose first convolutions was calculated along a significantly different direction than the direction perpendicular on the angular convolution. This results in a low-frequency artifact (bias). The severeness of this artifact is dependent on the width of the Gaussian function.

k large (far from the origin)

If k is large compared to the width of the Gaussian function, then

$$\frac{\epsilon_{max}}{k} \ll 1. \tag{7}$$

Expansion of $\frac{k}{\sqrt{k^2+\epsilon^2}}$ and $\frac{\epsilon}{\sqrt{k^2+\epsilon^2}}$ yields

$$\begin{aligned}\frac{k}{\sqrt{k^2+\epsilon^2}} &\approx 1+O\left(\frac{\epsilon}{k}\right)^2 \\ \frac{\epsilon}{\sqrt{k^2+\epsilon^2}} &\approx 0+\frac{\epsilon}{k}+O\left(\frac{\epsilon}{k}\right)^3.\end{aligned} \tag{8}$$

so Eq. (6) becomes

$$\begin{aligned}F^{RA}(k\cos\theta, k\sin\theta) = \iint G(\epsilon)G(\epsilon')F\Big[&k\cos\theta-\epsilon\sin\theta-\epsilon'\cos\theta+\frac{\epsilon\epsilon'}{k}\sin\theta, \\ &k\sin\theta+\epsilon\cos\theta-\epsilon'\sin\theta-\frac{\epsilon\epsilon'}{k}\cos\theta\Big]\,d\epsilon\,d\epsilon'.\end{aligned} \tag{9}$$

We now perform the following coordinate transform:

$$\begin{aligned}t &= \epsilon\sin\theta+\epsilon'\cos\theta \\ t' &= -\epsilon\cos\theta+\epsilon'\sin\theta,\end{aligned}$$

which is in fact a rotation over angle $(\frac{\pi}{2}-\theta)$. Since a 2D spherical Gaussian function is rotation invariant, we have

$$G(\epsilon)G(\epsilon') = G(\epsilon,\epsilon') = G(t,t') = G(t)G'(t') \tag{10}$$

and Eq. (9) becomes

$$F^{RA}(k\cos\theta, k\sin\theta) = \iint G(t)G(t')F(k\cos\theta-t+R_1, k\sin\theta-t'+R_2)dt\,dt' \tag{11}$$

with

$$\begin{aligned}R_1 &= t^2\frac{\sin^2\theta\cos\theta}{k}-tt'\frac{\sin\theta\left(\sin^2\theta-\cos^2\theta\right)}{k}+t'^2\frac{\cos\theta\sin^2\theta}{k} \\ R_2 &= -t^2\frac{\sin\theta\cos^2\theta}{k}+tt'\frac{\cos\theta\left(\sin^2\theta-\cos^2\theta\right)}{k}-t'^2\frac{\cos^2\theta\sin\theta}{k}.\end{aligned}$$

A Taylor expansion of F about $(k\cos\theta-t, k\sin\theta-t')$ results in

$$\begin{aligned}F^{RA}(k\cos\theta, k\sin\theta) &= \iint G(t)G(t')F(k\cos\theta-t, k\sin\theta-t')dt\,dt' \\ &\quad+\iint G(t)G(t')R_1\frac{\partial F(k\cos\theta-t, k\sin\theta-t')}{\partial(k\cos\theta-t)}dt\,dt' \\ &\quad+\iint G(t)G(t')R_2\frac{\partial F(k\cos\theta-t, k\sin\theta-t')}{\partial(k\sin\theta-t')}dt\,dt' \\ &= F(k\cos\theta, k\sin\theta)*[G(k\cos\theta)*G(k\sin\theta)] \\ &\quad-\iint G(t)G(t')R_1\frac{\partial F(k\cos\theta-t, k\sin\theta-t')}{\partial t}dt\,dt' \\ &\quad-\iint G(t)G(t')R_2\frac{\partial F(k\cos\theta-t, k\sin\theta-t')}{\partial t'}dt\,dt'.\end{aligned} \tag{12}$$

Performing partial integration and noticing that $G(t)$, $G(t')$ and $F(k\cos\theta - t, k\sin\theta - t')$ are zero at $-\infty$ and ∞, Eq. (12) becomes

$$\begin{aligned} F^{RA}(k\cos\theta, k\sin\theta) &= F(k\cos\theta, k\sin\theta) * [G(k\cos\theta) * G(k\sin\theta)] \\ &\quad - \iint G(t')F(k\cos\theta, k\sin\theta)\left[[R_1\frac{\partial G(t)}{\partial t} + G(t)\frac{\partial R_1}{\partial t}\right] dt\,dt' \\ &\quad - \iint G(t)F(k\cos\theta, k\sin\theta)\left[[R_2\frac{\partial G(t')}{\partial t'} + G(t')\frac{\partial R_2}{\partial t'}\right] dt\,dt' \end{aligned} \tag{13}$$

$$\begin{aligned} &= F(k\cos\theta, k\sin\theta) * [G(k\cos\theta) * G(k\sin\theta)] \\ &\quad + \left[\frac{\sin^2\theta\cos\theta}{k\gamma^2}F(k\cos\theta, k\sin\theta)\right] * \left[k^3\cos^3\theta\, G(k\cos\theta) * G(k\sin\theta)\right] \\ &\quad - \left[\frac{\cos^2\theta\sin\theta}{k\gamma^2}F(k\cos\theta, k\sin\theta)\right] * \left[G(k\cos\theta) * k^3\sin^3\theta\, G(k\sin\theta)\right] \\ &\quad - \left[\frac{\sin^3\theta}{k\gamma^2}F(k\cos\theta, k\sin\theta)\right] * \left[k^2\cos^2\theta\, G(k\cos\theta) * k\sin\theta\, G(k\sin\theta)\right] \\ &\quad + \left[\frac{\cos\theta(2\sin^2\theta - \cos^2\theta)}{k\gamma^2}F(k\cos\theta, k\sin\theta)\right] * \left[k\cos\theta\, G(k\cos\theta) * k^2\sin^2\theta\, G(k\sin\theta)\right] \\ &\quad + \left[\frac{\cos\theta}{k}F(k\cos\theta, k\sin\theta)\right] * [k\cos\theta\, G(k\cos\theta) * G(k\sin\theta)] \\ &\quad + \left[\frac{\sin\theta}{k}F(k\cos\theta, k\sin\theta)\right] * [G(k\cos\theta) * k\sin\theta\, G(k\sin\theta)], \end{aligned} \tag{14}$$

with γ the width of the Gaussian function. The first term in this equation represents a convolution of the Fourier transformed object density function $F(k\sin\theta, k\cos\theta)$ and a 2D Gaussian filter $G(k\cos\theta) * G(k\sin\theta) = G(k\cos\theta, k\sin\theta)$. This term is exactly what we want. The other terms describe deviations (small for large k) from this result.

2.3. Filter

The second cause of artifacts is the place of the first filtering in the algorithm. In order to avoid interpolation in the frequency space to calculate the angular convolution, we reconstruct the image and then we reproject it while multiplying with the Gaussian window function. This means that there is already a non-local filtering part in the algorithm, before the full 2D convolution is done. The result is again a bias, because the filtering is still a non-local operation on truncated projections. But as mentioned above, the bias is smaller when less dense structures surround the ROI. In this case, we multiplied the truncated projections with a 1D Gaussian function, so that the weight of the structures outside the ROI becomes smaller, which corresponds with lower densities. Thus the effect of this filtering is significantly smaller than it would be without the algorithm. The numerical simulations on a phantom will show whether this artifact is small enough.

2.4. Practical considerations

A general approach to incomplete data problems is data completion. The algorithm presented here can be combined with mathematical extrapolation of the data in the missing range. The most important reason is to cope with boundary problems at the edges of the truncated projections. There have been several studies on extrapolations, but in this work we only investigate a few simple estimates (0^{th} order, 1^{st} order and $\cos^2$) in this work. The most satisfying extrapolation seems to be the $\cos^2$ extrapolation because of its mean squared error (MSE)[‡] stability for edges in the object (the MSE doesn't vary much when the edge of the ROI corresponds to

[‡] $MSE(f'(x,y)) = \sum_{x,y}\left(f'(x,y) - f(x,y)\right)^2$ with $f'(x,y)$ and $f(x,y)$ the calculated and the real object function, respectively.

a high gradient in the object function). In our experiment, the truncated projections are extrapolated with a $\cos^2$ function,

$$P_\theta(t) = \begin{cases} 0 & if\ t \in [-\infty, -b] \\ P_\theta(-a)\cos^2\left(\frac{t+a}{b}.\frac{\pi}{2}\right) & if\ t \in [-b, -a] \\ P_\theta(t) & if\ t \in [-a, a] \\ P_\theta(a)\cos^2\left(\frac{t-a}{b}.\frac{\pi}{2}\right) & if\ t \in [a, b] \\ 0 & if\ t \in [b, \infty]\,, \end{cases} \tag{15}$$

with $2b$ and $2a$ the size of the object and ROI respectively. Then we reconstruct the image by applying the

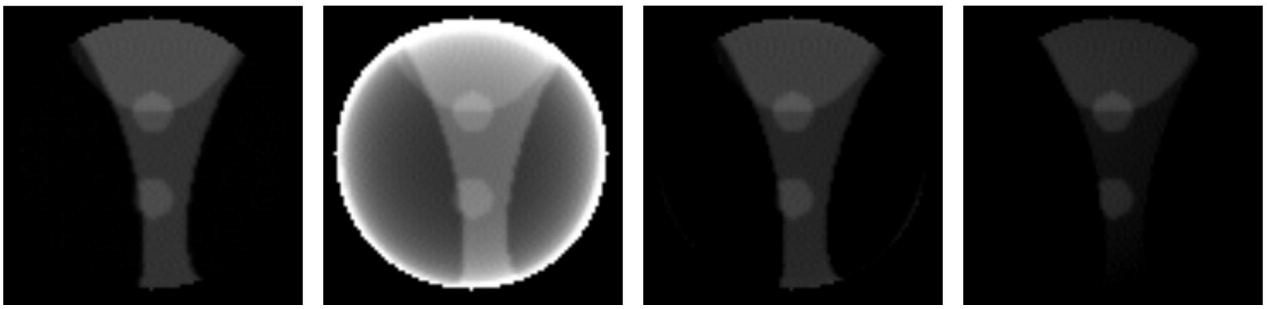

(a) reference (b) no extrapolation (c) zero order extrapolation (d) 1^{st} order extrapolation

(e) $\cos^2$ extrapolation

Figure 4. Qualitative comparison of some extrapolations

ROI-reconstruction algorithm.

For implementation simplicity and in order to speed up the algorithm, the weighted reprojection (step 3) and further operations are implemented differently, so the algorithm becomes:

1. Multiply every projection with a 1D Gaussian function (see figure 2.1. a)
2. Reconstruct the object with FBP.
3. Multiply with a 2D Gaussian function.
4. Reproject (Radon Transform).
5. Divide the projections by a 1D Gaussian function along the projections.
6. Reconstruct performing FBP.
7. Divide the reconstruction by the 2D Gaussian function.

.

3. RESULTS AND DISCUSSION

In following discussion, the MSE is chosen as quality criterium. This means that the bias has a high weight in comparison with that of the precision which accords to our goal to allow quantitative analysis of ROI CT-images. We examine the dependence of the MSE of a reconstruction, on the width of the Gaussian function and on an extra margin of pixels (Region Of Exposure, ROE) surrounding the ROI. These results are compared with the reconstruction from the projections by applying the usual FBP algorithm. In figure 5 the MSE's of these reconstructions are plotted in function of the width of the Gaussian (unit is the width of ROI). The different curves represent reconstructions with different ROE. The reference for the MSE is the FBP reconstruction from the *full* projections.

The straight lines in the figure represent the MSE of the reconstruction from the truncated and extrapolated projections with the FBP method, so the parts of the curves below these lines represent the Gaussian functions that produce better reconstructions than without the algorithm. An interesting observation is that a critical Gaussian width can be found for which the algorithm reaches a MSE that is often more than five, and sometimes more than ten times smaller than without the algorithm. Moreover, there is a large range for which the algorithm is useful. The MSE explodes for smaller Gaussian widths because then a larger region in frequency space will be affected by the fact that the second convolution is incorrectly calculated on values that are already the result from convolutions in different directions (see 2.2: Discussion). We also notice that the useful range does not necessarily overlap with ranges of other objects, ROE's or ROI's. The next step is now to find this interesting critical value and range for an unknown object.

An example of the quality improvement using the Gaussian algorithm is given in figure (6). We observe a significant diminution of the bias.

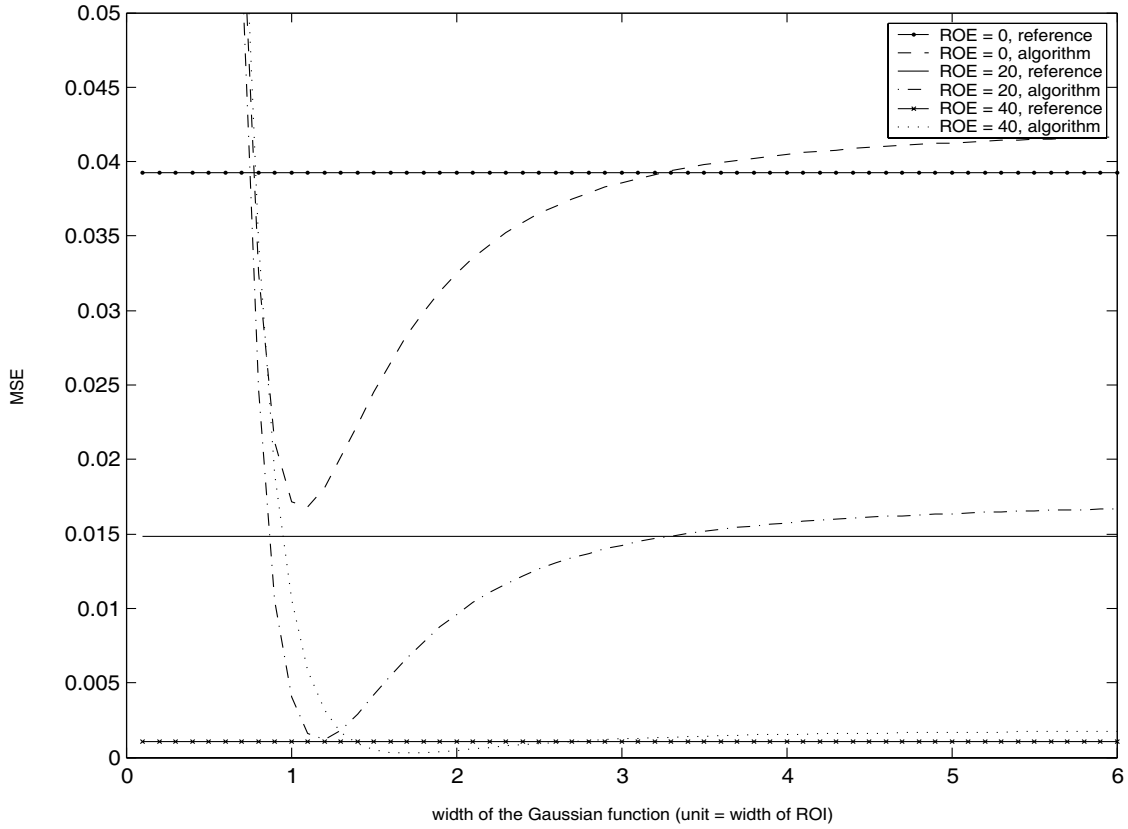

Figure 5. result of the algorithm for the 256×256 phantom showed in fig. 6 (a) with a centered ROI of 60 pixels

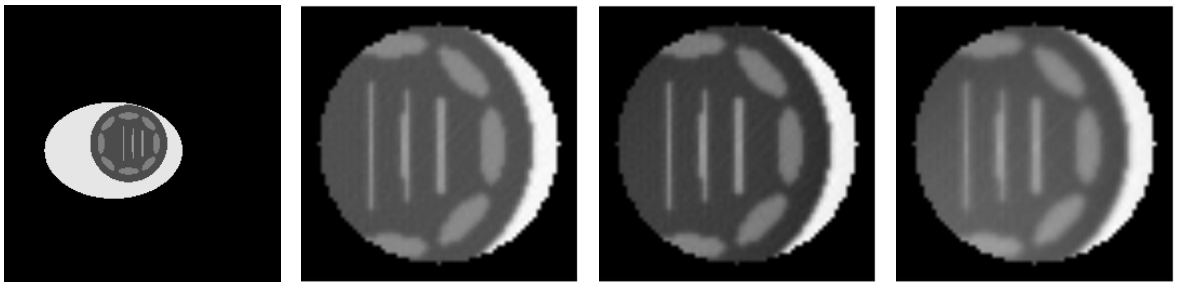

(a) (b) (c) MSE = 0.039 (d) MSE = 0.017

Figure 6. (a) is the used phantom, (b) is the reference reconstruction. (c) and (d) are the respective reconstructions from truncated projections without and with use of the algorithm.

4. CONCLUSIONS AND FURTHER DEVELOPMENT

In this paper, we present a general method for ROI tomography that makes use of a Gaussian window and reduces the amount of radiation significantly. The method is applicable to various objects and doesn't need a priori information about the object. For an optimal choice of Gaussian width and region of exposure, the proposed method gives improved approximations. In a next stage, the method will be extended to realistic 3D cone-beam scanning configurations, for which it will be combined with the filtered backprojection based Feldkamp algorithm [1]. The most important goal is then to reduce the transaxial (plane of source) contamination of the structures surrounding the ROI.

REFERENCES

1. L.A.Feldkamp, L.C.Davis and J.K.Kress. Practical cone-beam algorithm. *Journal of the Optical Society of America*, 1984
2. A.Kak and M. Slaney. Principles of Computerized Tomographic Imaging. *SIAM, 2001*
3. F. Natterer. The Mathematics of Computerized Tomography, *SIAM,2001*
4. G. Tisson, P. Scheunders, D. Van Dyck. 3D Region of Interest X-Ray CT for Geometric Magnification from MultiResolution Truncated Projections. *IEEE International Symposium on Biomedical Imaging: Arlington, USA, April 2004*
5. R.M.Lewit and R.H.T. Bates, Image reconstruction from projections: III: Projection completion methods. *Optik 50, 1978, No.3, 189-204*
6. S. Azevedo, P. Rizo, P. Grangeat, Region-of-Interest Cone-Beam Computed Tomography, *International Meeting on Fully Three-Dimensional Image Reconstruction In Radiology and Nuclear Medicine, 1995*
7. T. Olson, J. DeStefano, Wavelet Localization of the Radon Transform. *IEEE Transactions on Signal Processing*, 42:8, 1994
8. A.H. Delaney, Y. Bresler, Multiresolution Tomographic Reconstruction Using Wavelets, *IEEE Transactions on Image Processing*, 4:6, 1995
9. B. Sahiner, A.E. Yagle, Region-of-Interest Tomography Using Exponential Radial Sampling, *IEEE Transactions on Image Processing*, 4:8, 1995
10. P.S. Cho, A.D.Rudd, R.H. Johnson, Cone-beam CT from width-truncated projections, *Computerized medical imaging and graphics*, 1996 Jan-Feb. 20(1). P 49-57.
11. F. Natterer, F. Wübbeling, Mathematical methods in image reconstruction, *SIAM, Monographs on Mathematical Modeling and Computation*, 2001